Research Article

SOHAG JOURNAL OF SCIENCES

https://doi.org/10.21608/sjsci.2023.205024.1075

Hydrothermally Synthesized Co- and Mg-doped CuO Nanostructures: Electrical and Dielectric Properties

H.A.A. Saadallah[a,*], A.M. Abdel Hakeem[a], S.A. Saleh[a,b], S. Hampel[c], E.M.M. Ibrahim[a]

[a] *Physics Department, Faculty of Science, Sohag University, Sohag-82524, Egypt*
[b] *Physics Department, College of Science & Arts, Najran University, P.O. 1988, Najran, Saudi Arabia*
[c] *Leibniz Institute of Solid State and Material Research Dresden, P.O. Box 270016, D-01171 Dresden, Germany*
**E-mail: hany.saadallah@science.sohag.edu.eg*

Received: 15th April 2023, **Revised:** 5th May 2023, **Accepted:** 10th May 2023
Published online: 12th May 2023

Abstract: Herein, Co- and Mg-doped CuO nanostructures have been hydrothermally synthesized. The X-ray diffraction technique has been employed for investigating the phase purity and crystal structure, where formation of a typical single phase monoclinic CuO structure has been confirmed. Sharp and intense diffraction peaks have been observed and indicate to a high degree of crystallinity of the synthesized samples. No indication to any secondary or impurity phases could be observed. Microscopic investigation has been used to figure out the size, shape and surface morphology. Both samples show flakes-like nanostructure, with thickness ranging from 30 to 50 nm and from 40 to 100 nm for Co- and Mg-doped CuO respectively. The dielectric properties of the prepared samples have been investigated and compared through examining the frequency dependence of various dielectric parameters and the electrical behavior has been explained. Also, the conductivity and the dielectric parameters have been studied with variation in temperature.
Keywords: CuO nanostructures; hydrothermal; dielectric; electrical properties

1. Introduction

Transition Metal Oxide (TMO) nanostructures (NSs) have been the focus of technological developments in nanoscience for many years and have attracted more attention and research interest in the scientific community because of their unusual characteristics including availability, low cost, wider chemical reactivity, less toxicity, high chemical and thermal stability. Because of these advantages they are used in different applications for example electrochemical supercapacitors, gas sensors, photocatalytic and biomedical applications [**1-4**]. CuO as a TMO has enormous interest because of the unique properties such as easy synthesis method, low cost, nontoxicity and abundantly available constituents. CuO is a monoclinic p-type TMO. Many research groups have lately a great deal of interest in p-type TMO NSs because of their fascinating physicochemical characteristics, which make them promising multi-functional materials [**5**].

Because of these specific features, the CuO NSs with tuned structural, and optoelectronic properties are employed in a variety applications including antibacterial **[6, 7**], photoelectrodes [**8**], gas sensors [**9, 10**], memory devices [**11**], solar water-splitting [**12**], photocatalyst [**13, 14**], water treatment [**15**], supercapacitors [**16**], solar cells [**17, 18**], Li–ion batteries [**19-21**] etc.

Many techniques are used to synthesize CuO NSs with various morphologies such as chemical precipitation method [**21, 22**], sol gel [**23, 24**] and hydrothermal [**7, 25**]. The main focus on these methods because simplicity, low synthesis temperature and one can produce single and multi-phases materials. Hydrothermal synthesis is one of the most commonly used techniques for synthesis of nanomaterials It shows the following advantages: (i) water is non-toxic, low- cost and environment friendly (ii) water has strong polarity that motivates the oriented growth of nanocrystals (iii) many inorganic salts are easily dissolvable in water giving the possibility to choose the source of the metal ions as needed. [**5**]. Through experimental studies, it has been confirmed that the cupric source type and concentration, reaction time, temperature and pH value of the medium have a significant impact on the crystal growth direction, particle sizes and morphologies of the final product of the CuO nanostructure and thus tailoring of optical, magnetic, and electrical properties can be achieved **[5, 26**].

Both the dopant type and concentration are effective routes to expand the area of applications of CuO NSs through tuning the structural, and optoelectronic properties. Many metal atoms such as Cr, Zn, Fe, Al, Ni, Mn, Na and Co have been employed as dopants to tune the physical properties of CuO **[11, 16, 21, 27-31**].

Dielectric study is very important and valuable tool for understanding the transport behavior of ions in solid state ionic conductors. Sufficient information concerning translational and orientational movement of the mobile charge carriers found in the dielectric systems can be provided through the dielectric study. The complex permittivity varies with the applied electric field's frequency and is influenced by the physical characteristics of the materials. The variation of the complex permittivity in different frequency range originated as a result of various dielectric polarization types including electronic, ionic, orientational and interfacial etc. Alternating current (AC) conduction technique is widely used to understand the electrical

properties of a material and it can be utilized to identify the conduction mechanism of a dielectric materials.

The electrical performance of CuO can be affected by various parameters such as the chemical composition, preparation method and morphology. In this study, Co- and Mg-doped CuO NSs are successfully synthesized using the hydrothermal method. The structural, electrical, and dielectric properties are studied. The dielectric properties are studied through measuring different parameters as functions in frequency and temperature. The AC and DC conduction mechanisms are identified and well discussed.

2. Materials and methods

2.1. Chemicals

The precursors used for the preparation of Mg- and Co-doped CuO NSs are copper nitrate trihydrate [$Cu(NO_3)_2{\cdot}3H_2O$] (LOBA chemie 99.5%), magnesium nitrate hexahydrate [$Mg(NO_3)_2{\cdot}6\,H_2O$] (Alpha Chemicals 99%), cobalt nitrate hexahydrate [$Co(NO_3)_2{\cdot}6\,H_2O$] (Sigma Aldrich ≥ 98%) and sodium hydroxide [NaOH]. Double distilled water was used as a solvent. All chemicals and solvents are of analytical reagent grade. The crystallinity of the samples was investigated using x-ray diffractometer (XRD, Bruker D8-Advance) with Cu-Kα radiation source (λ=1.5406 Å). The XRD diffractograms were recorded within a diffraction angle 2θ range from 20° to 80°. The Field Emission-Scanning Electron Microscope FE-SEM (ZEISS-Sigma 500 FE-SEM) was utilized to investigate the surface morphology, particle shape and size as well as particle size distribution. The AC conductivity, loss factor and dielectric constant were measured using IM 3536 LCR Meter HIOKI.

2.2. Synthesis of Mg- and Co-doped CuO nanostructures

To synthesis $Cu_{0.94}A_{0.06}O$ (A=Mg and Co) NSs by hydrothermal method, at first, (0.025 moles.L^{-1}) copper nitrate trihydrate was magnetically stirred for 15 min at 50 °C to completely dissolve copper nitrate into double distilled water. Then magnesium nitrate hexahydrate salts with the concentration (x=0.06) was added to the copper nitrate solution. After that, NaOH solution was added as drops until reaching pH = 13 with maintaining the solution under continuous stirring at 50 °C for 30 min. Then, the solution was charged in an autoclave and inserted into a muffle furnace at 170 °C for 48 h (reaction time). After terminating of the reaction time, the autoclave was cooled naturally to room temperature. The black obtained precipitate was cleaned with distilled water and ethanol and dried at 100 °C for 2 h in air, then sintered at 350 °C for 2 hours. Co-doped CuO nanostructures was prepared in the same procedures by replacing [$Mg(NO_3)_2{\cdot}6H_2O$] by [$Co(NO_3)_2{\cdot}6H_2O$] for reaction time 24 h.

3. Results and Discussion:

3.1. Structural analysis

The structure, crystallinity and phase purity of the Mg- and Co-doped CuO samples was investigated using XRD technique. Fig. 1 displays the XRD reflections of the two synthesized samples beside that of the pure CuO for comparison. The sharp reflections observed at crystallographic planes (110), (11$\bar{1}$), (111), ($\bar{1}$12), (20$\bar{2}$), (020), (202), ($\bar{1}$13), (31$\bar{1}$), (220), (311) and (004) coincide with the COD (9016105) data of the monoclinic CuO pure phase. Also, comparison exhibits well match with many previously published work **[11, 32]**. Sharp and intense reflections can be observed and indicate to a high degree of crystallinity of the synthesized samples. No indication to any secondary or impurity phases could be observed because the dopants concentration is under the solubility limits [**33**]. The XRD results confirm that Mg and Co atoms replace the Cu atoms in the CuO lattice without any change in the monoclinic structure.

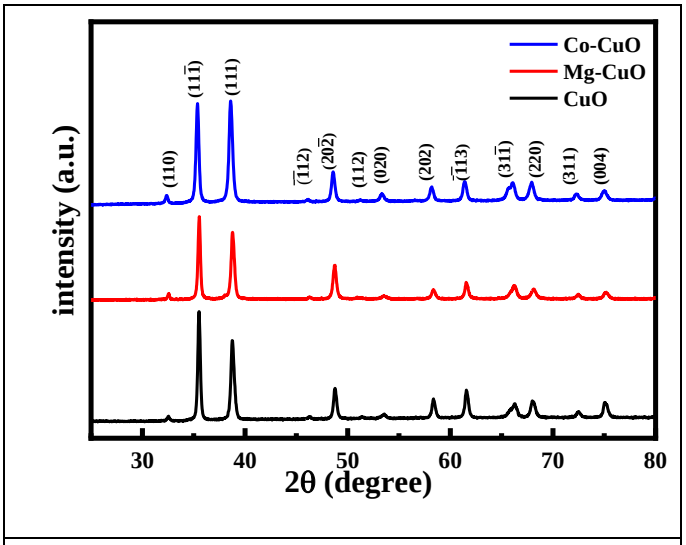

Fig. 1. The XRD patterns of $Cu_{0.94}Mg_{0.06}O$ and $Cu_{0.94}Co_{0.06}O$ nanostructures.

The values of the lattice parameters (a, b, c and β) and the cell volume (V) of the monoclinic system was calculated using the equations **[34]**:

$$\frac{1}{d^2}=\frac{1}{\sin^2\beta}\left(\frac{h^2}{a^2}+\frac{k^2\sin^2\beta}{b^2}+\frac{l^2}{c^2}-\frac{2hl\cos\beta}{ac}\right) \quad (1)$$

$$V=abc\sin\beta \quad (2)$$

where d and (h, k, l) are the inter planer distance and miller indices for the reflection peaks, respectively. Also, the values of the lattice parameters (a, b, c and β) have been found to be in a good match with the standard values **[11, 16, 32, 35-37]**. Based on the fact that the variation of (c/a) ratio represents the structural deformation of the material, it can be observed from Table 1 that the calculated values of a/b, c/b ratios and β are nearly the same, indicating that incorporation of Mg or Co atoms into CuO lattice has similar effect on the lattice deformation.

The crystallite size (D) is estimated from the dominant diffraction peak (11$\bar{1}$) using the well-known Scherer's equation [**32**]:

$$D=\frac{K\lambda}{\beta_{hkl}\cos\theta} \quad (3)$$

where K= 0.9 , λ, β_{hkl} and θ are the shape factor, wavelength of the x-ray beams (1.5406 Å), full width at the half maximum (FWHM) and diffraction angle respectively.

The dislocation density (δ) of the Mg- and Co-doped CuO NSs was calculated using the following relation [**35**]:

$$\delta = \frac{1}{D^2} \quad (4)$$

Because of the large fraction of surface atoms and unsaturated dangling bonds which are responsible for many unusual physical and chemical properties of nanomaterials, an internal strain is raises. In this study, the internal strain (η) was estimated using the following relation [24, 29, 36]:

$$\eta = \frac{\beta_{hkl} \cos\theta}{4} \quad (5)$$

The data tabulated in Table1 indicates that Mg-doped CuO and Co-doped CuO samples have approximately the same lattice parameters and cell volume values but different η and δ which can be attributed to the difference between the atomic radius of Mg (160 pm) and Co (126 pm) that results in a difference in the lattice strain and dislocations content.

	Mg-CuO	Co-CuO
a (Å)	4.685 ± 0.00234	4.700 ± 0.0244
b (Å)	3.420 ± 0.00156	3.414 ± 0.00145
c (Å)	5.128 ± 0.00305	5.106 ± 0.0285
a/b	1.370	1.377
c/b	1.499	1.496
β	99.530 ± 0.045	99.362 ± 0.044
V (Å ^{3})	81.029 ± 0.072	80.885 ± 0.070
D (nm)	57.1± 0.05	35.51± 0.03
$\delta \times 10^{-4}$ (line/nm^2)	3.07± 0.03	7.93± 0.07
$\eta \times 10^{-4}$	6.07± 0.06	9.73± 0.09

Table 1: The 2θ value, lattice parameters, crystal size (D), dislocation density (δ) and internal strain (η) of the Mg and Co doped CuO NSs samples.

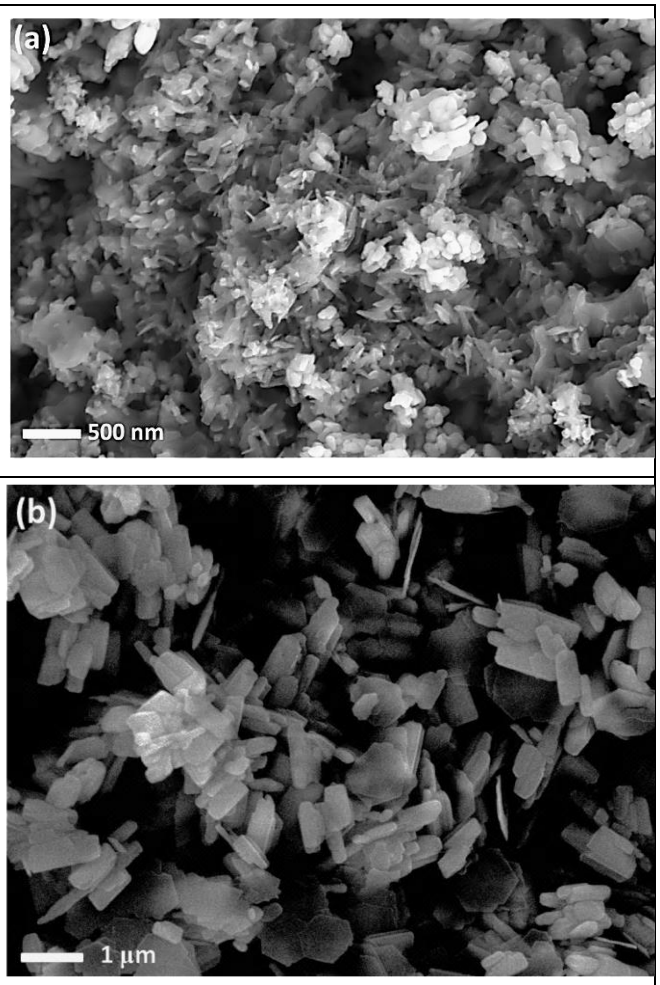

Fig: 2. SEM images for (a) Co- and (b) Mg-doped CuO nanostructures respectively.

3.2. Morphological study

Fig. 2 shows the SEM images of the Mg- and Co-doped CuO samples. Both samples show flakes-like nanostructure. Size distribution analyses indicates that the Mg-doped CuO nanoflakes size is in sub-micrometric scale with thickness ranging from 40 to 100 nm while the Co-doped CuO nanoflakes show smaller size with thickness ranging from 30 to 50 nm. The results coincide with the results of the XRD analyses were crystallite size D of Co-doped samples (D=35.51 nm) is much lower than that of Mg-doped sample (D=57.1 nm).

3.3. The electrical study

3.3.1. AC conductivity (σ_{AC})

Fig. 3a shows the variation of the total conductivity (σ) of the Co- and Mg-doped CuO nanostructures with frequency (ω) measured at room temperature. The total conductivity is represented by the relation [38] :

$$\sigma = \sigma_{dc}(T) + \sigma_{ac}(\omega, T) \quad (6)$$

According to Eq.6, the total conductivity σ is the sum of the DC conductivity (σ_{dc}) and AC conductivity (σ_{ac}). Contribution of any of the two conduction mechanisms depends on many factors such as the frequency of the applied field, ambient temperature, energy of charge carriers [39], etc. As seen in Fig.3a, each ln(σ) vs. ln (ω) plot consists of two regions [14, 36]: (I) plateau region at the lower frequencies which denotes the contribution of σ_{dc} where the conductivity is frequency independent and related to the long–range motion of the free charge carriers. (II) The dispersion region, which characterizes the higher frequency region where the contribution of the σ_{ac} to the total conductivity increases as the frequency increases. Fig. 3b & c illustrates the total conductivity (σ) versus frequency (ω) plots measured at various temperatures. The figures show that σ increases with increasing the temperature as a result of the increase in the charge carriers and thermal agitation suggesting a semiconductor behavior of the materials [14]. It is also observed that the width of the plateau region increases with increasing the temperature and shifts to higher frequencies where the hopping frequency is that frequency at which the behavior changes from the DC to AC conductivity [40-42].

3.4. Dielectric Study

Studying the dielectric features of a material gives important information about the dominant polarization type, mechanisms of the electrical conduction and dielectric relaxation. It is important to mention that permittivity is not constant but varies with the orientation and molecular structure mixture, pressure of the material, the applied frequency and temperature. The complex permittivity (ε*) is given by the equation [43, 44]:

$$\varepsilon^* = \varepsilon' - j\varepsilon'' \quad (7)$$

where ε′ (the real part of the complex permittivity) describes the energy stored in the dielectric material as polarization. ε″ (the imaginary part of the complex permittivity) describes the energy dissipated as heat. ε′ and ε″ are related by the loss tangent, tanδ [45]:

$$\varepsilon'' = \varepsilon' \tan\delta \quad (8)$$

3.4.1. Dielectric constant (ε')

Fig. 4a shows the variation of the real part (ε′) of the Co- and Mg-doped CuO nanoflakes with (ω) measured at room temperature. Notably, ε′ decreases as the frequency increases reaching a constant value in the high frequency range. Fig. 4b & c shows ε′ vs. ω plots measured at different temperatures. Similar behavior have been observed for all the samples where, ε′ always decreases as ω increases whatever the measurement temperature is but it increases with increasing the temperature. At first, it should be known that the dielectric behavior and the polarizability of a material are related to each other, so in order to understand the dielectric behavior we must understand the polarizability of a material more deeply. Usually for the polar materials, the overall polarizability of a material is attributed to the contribution of multi-component polarization mechanisms such as electronic, ionic, space charge and orientational polarization [34, 45]. The main contribution to the total polarizability (within the frequency range of measurements in this work) comes from the Rotation Direction Polarization (RDP) and Space Charge Polarization (SCP) [46-48]. RDP is formed at the interfaces in nanostructures when oxygen vacancies generate a large number of rotated dipole moments under the applied field. The SCP results from a high number of defects (oxygen vacancies). The electrostatics theory states that the charges at the interfaces are attracted by the opposite poles of the electric field and are mostly trapped by defects. This leads to the development of dipole moments, which in turn leads to the polarization of the space charge. As a result, the observed high ε′ at low frequencies for the samples under study is due to both RDP and SCPs contribution. Back to Fig.4, the samples under study exhibit relatively high ε′, particularly at high temperatures and low frequencies. In the high frequency region, ε′ becomes approximately constant where all the curves merge irrespective of the ambient temperature. The dipoles' contribution to polarization and the dielectric constant is weak at low temperatures and high frequencies because they are rigidly fixed and unable to follow and orient themselves along the applied field. The observed increase in ε′ with temperature is due to the increase in the degree of freedom of movement of the dipoles. Also, at high temperatures, the thermal energy of the bound dipoles become enough to enable them to follow the change in the external field easily [45].

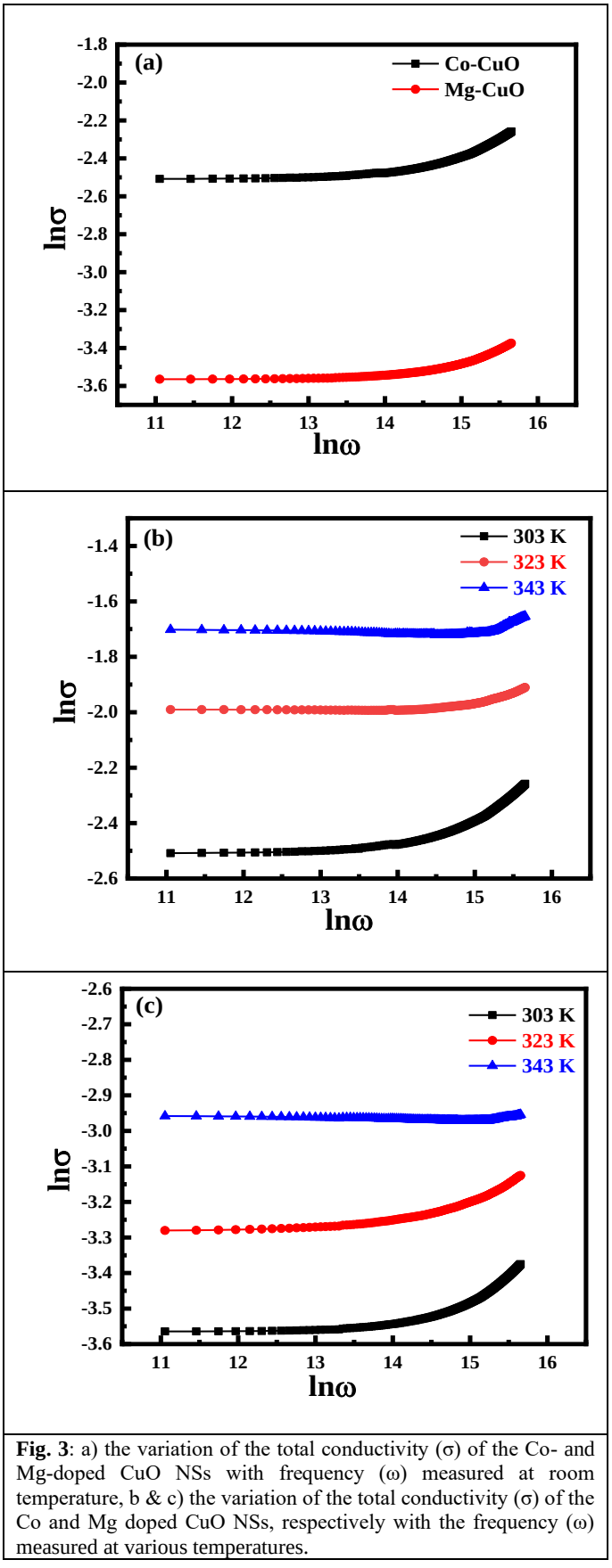

Fig. 3: a) the variation of the total conductivity (σ) of the Co- and Mg-doped CuO NSs with frequency (ω) measured at room temperature, b & c) the variation of the total conductivity (σ) of the Co and Mg doped CuO NSs, respectively with the frequency (ω) measured at various temperatures.

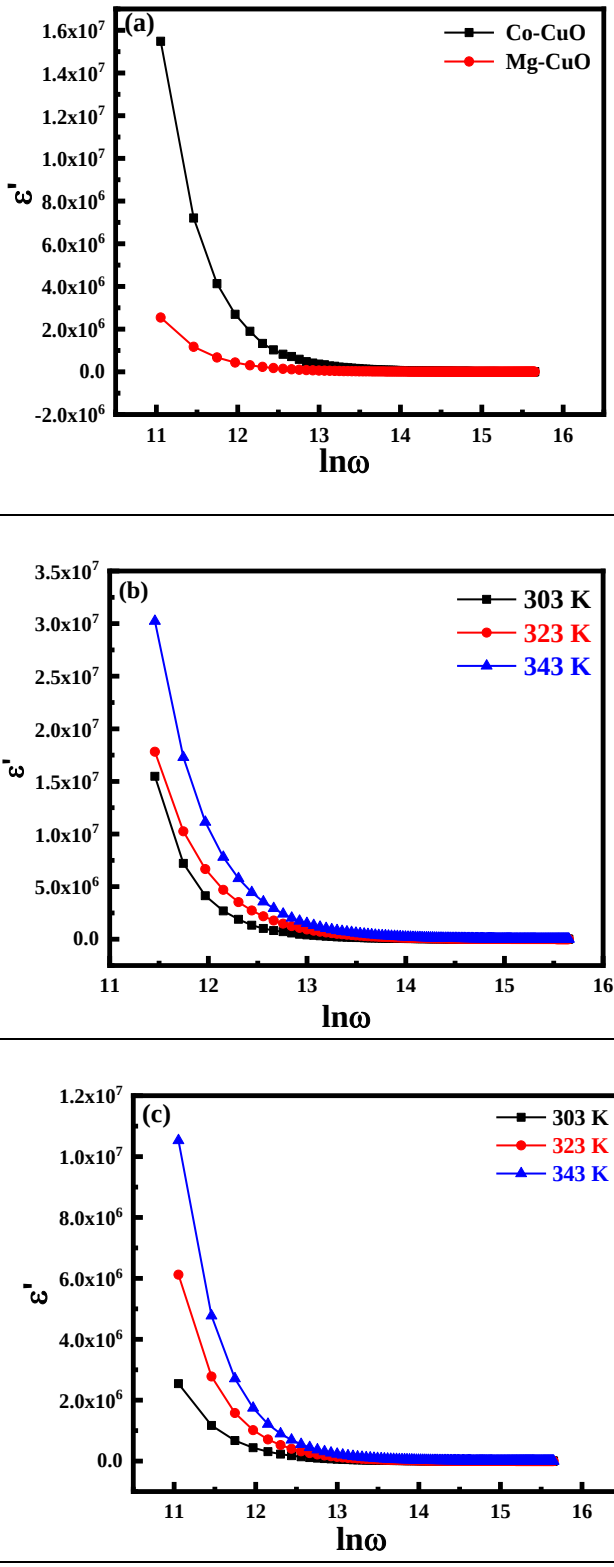

Fig. 4. Frequency (ω) dependency of the real permittivity (ε') of the Co-and Mg-doped CuO nanostructures with frequency (ω) (a) measured at room temperature, (b and c) measured at different temperatures, respectively.

Accordingly, the polarization increases leading to an increase in the dielectric constant. The overall behavior of the dielectric constant obeys the Maxwell–Wagner polarization model on the basis of Koops' theory **[49, 50]**.

According to Koops' model, the solid sample consists of good conducting grains, separated by low electric conductive grain boundaries. Consequently, when the movement charges carriers in the grain reaches the grain boundary of other its motion is perturbed. Thus, the charge carriers accumulate at the interface **[36, 45]** resulting in the increase of ε′. The nearly constant value of ε′ in the high frequency range indicates that the grain boundaries' contribution to ε' can be neglected compared to grain contribution **[36, 45]**. In particular, nanostructured materials contain large number of interfacial atoms and a large number of defects at the grain boundaries compared to their bulk materials [51]. As a consequence of the large number of defects, positive and negative space charge distribution is formed. These trapped charges at the interface generate space charge polarization [45]. The polarization occurs due to the large numbers of rotated dipole moments generated from the defects in the presence of the external field, where the nanostructures have a large surface area with a larger number of defects. As the frequency increases, the dipoles become unable to follow the electrical field and the orientation polarization disappears. Therefore, ε′ decreases to approximately a constant value representing the contribution of the interfacial polarization only.

3.4.2. Dielectric loss (ε″)

Fig. 5a displays the variation of imaginary part (ε″) of the complex permittivity with frequency (ω) of the Co- and Mg-doped CuO nanostructures measured at room temperature. The data imply that (ε″) decreases with increasing (ω) showing approximately a constant value in the high frequency region.

Fig. 4b & c displays ε″ vs. ω measured at different ambient temperatures. Similar behaviour have been observed for all the plots at different temperatures where ε″ decreases with increasing ω irrespective of the ambient temperature, while it increases as the temperature increases. As has been mentioned above, the dielectric loss is the energy loss as heat into the dielectric material with applying the electric field. The main reason for the emergence of ε″ is the delay of the response of the dipoles to the applied external field. The observed decrease in ε″ at low frequencies is due to the fact that the dielectric loss is caused by migration of ions in the material. However, in the moderate frequency range, ions polarization loss, conduction loss of ions migration and ions jump contributes to ε″. At high frequencies, ion vibrations are the only source of dielectric loss and thus, ε″ has the minimum value **[40, 46, 51]**. The increase of ε″ with temperature can be explained in the view of the three mechanisms of the relaxation phenomena: conduction loss, vibrational loss and dipole loss **[40, 45]**. At low temperatures, the conduction loss contribution shows a minimum value because it is proportional to σ/ω. By increasing temperature, σ increases due to the increase in the charge flow and so the conduction loss increases resulting in the increase of ε″. Also, by increasing the charge carriers flow, the polarization lag behind the applied field causing an interaction between the external field and the dielectric's polarizations which create an

additional electric field at the interface that distorts the externally applied field, which may lead to an increase in the dielectric loss. The formation of relaxation polarization takes long time and results in energy dissipation which leads to dielectric loss [45].

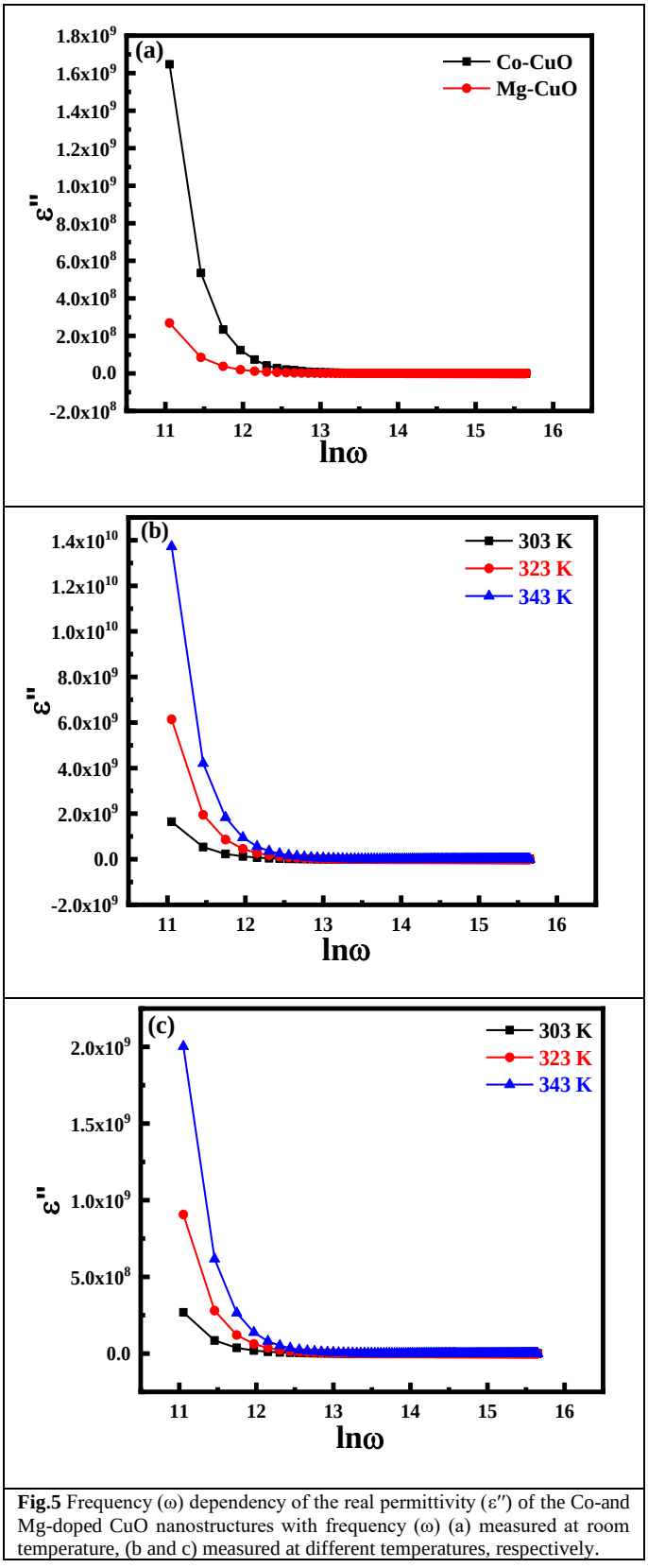

Fig.5 Frequency (ω) dependency of the real permittivity (ε″) of the Co-and Mg-doped CuO nanostructures with frequency (ω) (a) measured at room temperature, (b and c) measured at different temperatures, respectively.

4. Conclusion

In this work, the Co- and Mg-doped CuO NSs were successfully synthesized by hydrothermal method. The XRD results confirm that both samples are pure single phases without indication of any other phases. Microscopy investigations show that the synthesized samples have flakes-like structure and doping with Co and Mg has significant effect on the size of the CuO nanoflakes. Higher AC conductivity was found for Co-doped CuO sample compared to Mg-doped CuO sample, which may be attributed to the higher carrier concentration in the former. The variation of the dielectric constant and dielectric loss with frequency depend on the polarizability type that dominates in the material. The structural defects and grain boundary play important roles in the dielectric relaxation processes. The ambient temperature has a significant effect on the electrical and dielectric parameters of the materials under study. The obtained results candidate the materials under study for many promising applications such as gas sensor and energy storage capacitors.

References

[1] W.H. Low, P.S. Khiew, S.S. Lim, C.W. Siong, E.R. Ezeigwe, Journal of Alloys and Compounds, 775 (2019) 1324-1356.
[2] G. Maduraiveeran, M. Sasidharan, W. Jin, Progress in Materials Science, 106 (2019) 100574.
[3] J.M. Walker, S.A. Akbar, P.A. Morris, Sensors and Actuators B: Chemical, 286 (2019) 624-640.
[4] K. Kannan, D. Radhika, K.K. Sadasivuni, K.R. Reddy, A.V. Raghu, Advances in Colloid and Interface Science, 281 (2020) 102178.
[5] Q. Zhang, K. Zhang, D. Xu, G. Yang, H. Huang, F. Nie, C. Liu, S. Yang, Progress in Materials Science, 60 (2014) 208-337.
[6] T. Pandiyarajan, R. Udayabhaskar, S. Vignesh, R.A. James, B. Karthikeyan, Materials Science and Engineering: C, 33 (2013) 2020-2024.
[7] P. Kumar, M.C. Mathpal, J. Prakash, B.C. Viljoen, W. Roos, H. Swart, Journal of Alloys and Compounds, 832 (2020) 154968.
[8] J. Oh, H. Ryu, W.-J. Lee, Composites Part B: Engineering, 163 (2019) 59-66.
[9] R. Wahab, F. Khan, N. Ahmad, M. Alam, J. Ahmad, A.A. Al-Khedhairy, Colloids and Surfaces A: Physicochemical and Engineering Aspects, 607 (2020) 125424.
[10] G. Chaloeipote, R. Prathumwan, K. Subannajui, A. Wisitsoraat, C. Wongchoosuk, Materials Science in Semiconductor Processing, 123 (2021) 105546.
[11] B.P. Singh, M. Chaudhary, A. Kumar, A.K. Singh, Y.K. Gautam, S. Rani, R. Walia, Solid State Sciences, 106 (2020) 106296.
[12] S.W. Hwang, G.S. Han, J.Y. Cho, D.U. Lee, H.S. Han, I.S. Cho, Applied Surface Science, 585 (2022) 152632.
[13] S. Li, D. Chu, L. Wang, R. Rong, N. Zhang, Physica E: Low-dimensional Systems and Nanostructures, 126 (2021) 114489.

[14] C. Gherasim, P. Pascariu, M. Asandulesa, M. Dobromir, F. Doroftei, N. Fifere, A. Dascalu, A. Airinei, Ceramics International, 48 (2022) 25556-25568.
[15] J.O. Ighalo, P.A. Sagboye, G. Umenweke, O.J. Ajala, F.O. Omoarukhe, C.A. Adeyanju, S. Ogunniyi, A.G. Adeniyi, Environmental Nanotechnology, Monitoring & Management, 15 (2021) 100443.
[16] M. Chaudhary, M. Singh, A. Kumar, Y.K. Gautam, A.K. Malik, Y. Kumar, B.P. Singh, Ceramics International, 47 (2021) 2094-2106.
[17] D. Vikraman, H.J. Park, S.-I. Kim, M. Thaiyan, Journal of Alloys and Compounds, 686 (2016) 616-627.
[18] H. Siddiqui, M.R. Parra, P. Pandey, M. Qureshi, F.Z. Haque, Journal of Science: Advanced Materials and Devices, 5 (2020) 104-110.
[19] O. Waser, M. Hess, A. Güntner, P. Novák, S.E. Pratsinis, Journal of Power Sources, 241 (2013) 415-422.
[20] R. Zhang, J. Liu, H. Guo, X. Tong, Materials Letters, 139 (2015) 55-58.
[21] B. Heng, C. Qing, H. Wang, D. Sun, B. Wang, Y. Tang, Journal of Alloys and Compounds, 649 (2015) 899-905.
[22] T.A. Hameed, S. Yakout, M.A. Wahba, W. Sharmoukh, Optical Materials, 133 (2022) 113029.
[23] M. Bibi, H. Abbas, S. Baqi, Materials Chemistry and Physics, 192 (2017) 67-71.
[24] P. Chand, P. Kumar, Optik, 156 (2018) 743-753.
[25] B. Yuan, X. Liu, J. Liu, M. Li, D. Wang, Materials Letters, 236 (2019) 495-497.
[26] B.G. Mahmoud, M. Khairy, F.A. Rashwan, C.W. Foster, C.E. Banks, RSC advances, 6 (2016) 14474-14482.
[27] S. Bhuvaneshwari, N. Gopalakrishnan, Journal of Alloys and Compounds, 654 (2016) 202-208.
[28] M. Chandrasekar, M. Subash, S. Logambal, G. Udhayakumar, R. Uthrakumar, C. Inmozhi, W.A. Al-Onazi, A.M. Al-Mohaimeed, T.-W. Chen, K. Kanimozhi, Journal of King Saud University-Science, 34 (2022) 101831.
[29] R. Sirirak, P. Chaopanich, A. Prasatkhetragarn, C. Chailuecha, S. Kuimalee, A. Klinbumrung, Radiation Physics and Chemistry, 190 (2022) 109788.
[30] H. Siddiqui, M.R. Parra, M. Qureshi, M. Malik, F.Z. Haque, Journal of materials science, 53 (2018) 8826-8843.
[31] M.R. Islam, J.E. Obaid, M. Saiduzzaman, S.S. Nishat, T. Debnath, A. Kabir, Journal of Physics and Chemistry of Solids, 147 (2020) 109646.
[32] S. Kamble, V. Mote, Solid State Sciences, 95 (2019) 105936.
[33] B. Clavier, A. Zhadan, T. Baptiste, F. Boucher, A. Guiet, F. Porcher, V. Brezová, C. Roques, G. Corbel, Dalton Transactions, 51 (2022) 8411-8424.
[34] S.K. Kuanr, S. Nayak, K.S. Babu, Materials Science in Semiconductor Processing, 71 (2017) 268-274.
[35] R. Chandramohan, S. Valanarasu, V. Ganesh, M. Shkir, A. Kathalingam, S. AlFaify, Journal of Molecular Structure, 1171 (2018) 388-395.
[36] A. Pramothkumar, N. Senthilkumar, R.M. Jenila, M. Durairaj, T.S. Girisun, I.V. Potheher, Journal of Alloys and Compounds, 878 (2021) 160332.
[37] M. Jamal, S.S. Nishat, A. Sharif, Chemical Physics, 545 (2021) 111160.
[38] A.K. Jonscher, nature, 267 (1977) 673-679.
[39] J. Koshy, S.M. Soosen, A. Chandran, K. George, Journal of Semiconductors, 36 (2015) 122003.
[40] A. Zaafouri, M. Megdiche, M. Gargouri, Journal of alloys and compounds, 584 (2014) 152-158.
[41] S. Mohamed, M. Halimah, R. Subban, A. Yahya, Physica B: Condensed Matter, 602 (2021) 412480.
[42] Y. Ben Taher, A. Oueslati, N. Maaloul, K. Khirouni, M. Gargouri, Applied Physics A, 120 (2015) 1537-1543.
[43] I. Hodge, C. Angell, The Journal of Chemical Physics, 67 (1977) 1647-1658.
[44] H. Schütt, Solid state ionics, 72 (1994) 86-88.
[45] Ç. Oruç, A. Altındal, Ceramics international, 43 (2017) 10708-10714.
[46] K.T. Selvi, K.A. Mangai, M. Priya, S. Sagadevan, Physica B: Condensed Matter, 594 (2020) 412355.
[47] N. Abraham, S. Aseena, Materials Today: Proceedings, 43 (2021) 3698-3700.
[48] F. Ahmad, A. Maqsood, Materials Today Communications, 33 (2022) 104812.
[49] C. Koops, Physical review, 83 (1951) 121.
[50] T. Prodromakis, C. Papavassiliou, Applied Surface Science, 255 (2009) 6989-6994.
[51] Z. Wang, W. Zhou, L. Dong, X. Sui, H. Cai, J. Zuo, Q. Chen, Journal of Alloys and Compounds, 682 (2016) 738-745.